Evaluation of active control of a laminar separation bubble based on linear stability theory

By O. Marxen, R. B. Kotapati† AND D. You

1. Motivation and objectives

Control of laminar separation using zero-net-mass-flux (ZNMF) devices for airfoils operating at low to medium Reynolds numbers is a common approach in laboratory experiments, in both numerical (e.g., Fasel & Postl 2006; Rist & Augustin 2006) and experimental (e.g., Bons *et al.* 2001) setups. However, ongoing physical processes in such flows can be diverse, spanning from convective-type (Kelvin-Helmholtz) instability (Rist & Augustin 2006) to vortex-wall interaction (Simens & Jimenez 2006).

Here, an interpretation of a flow situation investigated numerically during the CTR summer program (Kotapati *et al.* 2006) in terms of local linear stability theory based on the Orr-Sommerfeld equation is presented. Such an instability corresponds to the convective-type Kelvin-Helmholtz instability for laminar separation bubbles (LSB). In contrast to Rist & Augustin (2006), the present flow possesses an actual ZNMF actuator geometry for forcing, and investigates a wider range of forcing frequencies.

Results obtained from numerical simulations mentioned above shall be post-processed and analysed with respect to unsteady disturbance evolution in the flow. First, stability characteristics of the different mean flows resulting from different forcing frequencies are evaluated theoretically; numerical data are then Fourier-analyzed in time and are compared to theoretical results. Based on such a comparison, a discussion of similarities and differences between numerical and theoretical results then allows us to conclude on physical mechanism in operation. This is expected to help to improve the efficiency of active flow-control devices in the future.

2. Flow configuration and mean flows

A configuration shall be considered that was studied numerically during the 2006 CTR summer program (Kotapati *et al.* 2006). Data from respective simulations (cases 2.2–2.5) in that reference shall be analyzed here with respect to their stability properties and disturbance evolution, leading to a deeper understanding of physical processes taking place in the controlled flowfields. A brief overview of the setup and the mean flow shall be given in this section. Note that the simulations are 2-D only. Nevertheless, in the following the term *transition* will be used, indicating saturation of the dominant disturbance, even though no true (3-D) turbulent state is reached.

2.1. *Overview*

The general setup is given by a finite flat plate with an elliptic nose placed in a channel with slip walls, subject to a uniform incoming freestream at the channel inlet. In the rear part of the plate, steady blowing and suction is applied on the upper (slip) wall of the

† Mechanical and Aerospace Engineering, The George Washington University, Washington, DC 20052, USA

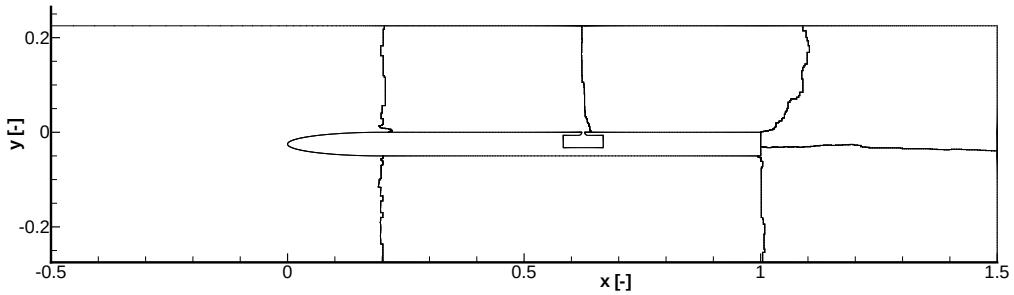

FIGURE 1. Configuration used for numerical simulations.

case	forcing frequency f_J
2.1	-
2.2	1.5
2.3	3.0
2.4	6.0
2.5	9.0

TABLE 1. Overview of simulation cases with respect to their forcing frequency.

channel in the interval $0.2 < x/c < 0.8$, which induces an adverse pressure gradient at the top wall of the flat plate and in turn leads to separation of the laminar boundary layer on that plate.

All quantities are non-dimensionalized with the inlet velocity of the channel and the chord of the plate. This amounts to a Reynolds number of 60,000. The wall-normal origin of the coordinate system lies on the top wall of the flat plate while the streamwise origin corresponds to the start of the plate, i.e., the (elliptic) nose. The flat part of the finite plate starts at x/c=0.2. In the following, we focus solely on the region around the separation bubble, which is located in the flat section downstream of the elliptic leading edge and upstream of the end of the plate, namely $0.2 < x/c < 1.0$.

A ZNMF actuator is centered at x/c=0.625. This actuator is used to diminish boundary-layer separation downstream of its location by forcing at different frequencies, but with a fixed amplitude. Four different non-dimensional frequencies were applied in the four different cases 2.2–2.5 (see Table 1). Case 2.1 refers to an undisturbed flow and will not be further considered.

The flow is computed by means of the second-order finite-volume based code CDP (Ham & Iaccarino 2004), which has been developed at the Center for Turbulence Research at Stanford University. For details of these simulations, refer to Kotapati *et al.* (2006). Only a very brief overview of the results with respect to the mean flow is provided in the next section. The mean flow for each case will be used as a base flow for subsequent stability calculations.

2.2. *Mean flows*

Figures 2 and 3 show boundary-layer parameters for all simulations with forcing. Those were computed from streamwise mean-flow velocity profiles up to a wall-normal distance of y=0.0347. Within this distance from the plate, changes in the potential flow, which introduce an error into the computation of displacement and momentum thicknesses, re-

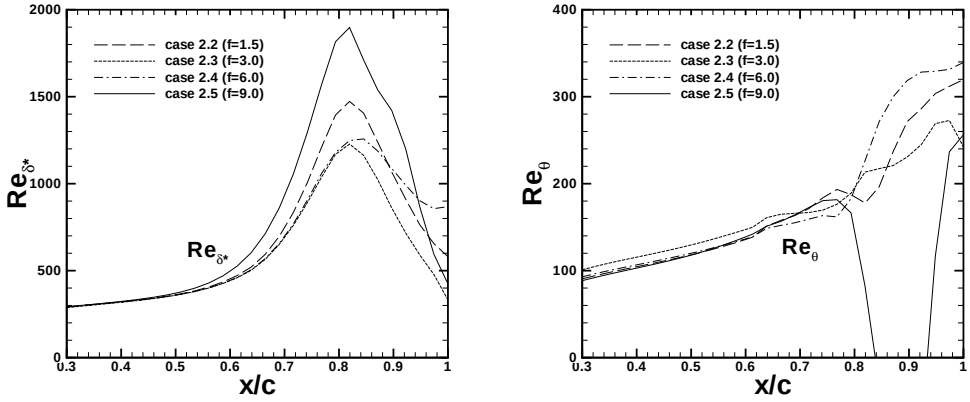

FIGURE 2. Reynolds numbers based on the displacement thickness δ_* (left) and the momentum thickness θ (right) for cases 2.2–2.5.

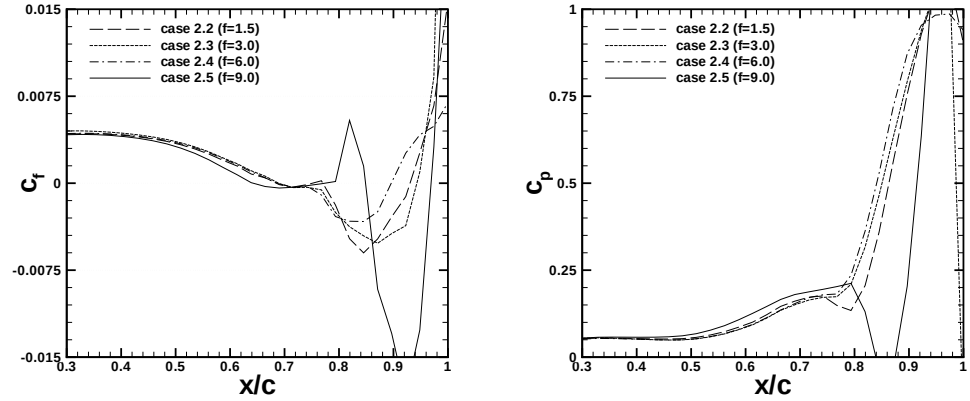

FIGURE 3. Skin-friction (left) and wall-pressure (right) coefficients for cases 2.2–2.5. The pressure is chosen such that it is the same for all cases at x/c=0.3.

main fairly small. Typical features of laminar separation bubbles can be observed when looking at these time-averaged quantities. For instance, the larger the bubble, the larger is its displacement thickness (see Fig. 2, left). The Reynolds number based on the momentum thickness θ (Fig. 2, right) strongly changes only when the flow transitions, so this quantity gives a rough idea of the transition location. The mean flow in case 2.5 (forcing frequency f=9) is somewhat similar to the undisturbed case (not shown here). Instead, case 2.5 will be referred to as essentially uncontrolled.

Forcing at the three lower frequencies ($f \leq 6$), cases 2.2–2.4 respectively, considerably reduces the size of the separation region. This is visible via the skin-friction coefficient c_f (Fig. 3, left), whose changes in sign from positive to negative and vice versa mark the separation and reattachment location, respectively. When compared to the essentially uncontrolled case 2.5 it is obvious that this reduction takes place from both sides, i.e., not only does the reattachment location move upstream, the separation location also

moves downstream. This is due to a feedback effect, namely disturbance input causes earlier transition downstream that in turn changes the mean flow, i.e., causes a mean flow deformation, via the pressure at the location of forcing or even upstream of it. Such a feedback effect of the mean flow deformation has also been reported by Marxen (2005).

This change in pressure due to forcing is clearly observable in Fig. 3 (right): the pressure increase is delayed upstream of transition, or more precisely disturbance input causes a weaker pressure increase upstream of separation, again in accordance with findings of Marxen (2005). Note that, for example, at x/c=0.6 the wall-pressure coefficient c_p possesses a larger value in case 2.3 or 2.4 than in case 2.5. Instead, on the downstream side, an earlier pressure increase takes place inside the separation bubble in cases 2.3 and 2.4 compared to case 2.5.

However, cases 2.2–2.4 possess essentially the same separation location, while slightly differing in mean reattachment location. This suggests that the reattachment processes are slightly different in these three cases, and that the upstream effect of the mean flow deformation does not always cause a simultaneous movement of both separation and reattachment location. On the other hand, when considering the pressure coefficient c_p (Fig. 3, right) it becomes clear that, for example, the pressure in case 2.2 is slightly higher upstream of separation at x/c=0.6 compared to case 2.4. This is in accordance with the fact that a slightly larger separation bubble has developed in case 2.2 with corresponding influence on the pressure distribution (the previously mentioned effect of the mean flow deformation).

In terms of size of separation bubbles, we would order them by increasing size (starting with the smallest) in the following way, based on the pressure distribution c_p and displacement Re_{δ^*}: case 2.4 (f=6), 2.3 (f=3), 2.2 (f=1.5), and 2.5 (f=9). The length of the separation bubble (computed from the skin-friction coefficient c_f) does not perfectly fit with this order, but a reason for that will be suggested below.

3. Linear stability theory: results for the different base flows and the effect of mean flow deformation

The development of perturbations introduced into a laminar flow via a ZNMF actuator is characterized by disturbance growth that will eventually lead to transition. For a sufficiently small disturbance level, the initial behavior of these perturbations is linear, i.e., can be treated by a set of linear equations, in contrast to the non-linear Navier-Stokes equations. Here, we will focus on a certain class of disturbances, specifically wave-like perturbations with exponential growth in x (spatial model).

A theoretical approach according to Schlichting (1979) is employed to describe the behavior of small disturbances: so-called Linear Stability Theory (LST) based on the Orr-Sommerfeld equation. Only a short overview of LST shall be given; more elaborate treatments can be found in Schmid & Henningson (2001) and Boiko *et al.* (2002). Decomposition of the flowfield into a known 2-D parallel steady base flow u_B=$u_B(y)$ (parallel-flow assumption) and small disturbance quantities s'=p', u', v', and linearizing with respect to these disturbances leads to a system of linear partial differential equations. Submitting a normal-mode ansatz for the perturbations:

$$s' = \check{s}' \cdot e^{i(\alpha x - \omega t)} + \text{conjugate complex}, \quad \check{s}' = \check{s}'(y) \in \mathbf{C}, \tag{3.1}$$

into the equations to obtain a separation of variables yields the Orr-Sommerfeld equation:

$$(\alpha\, u_B - \omega)\left(\frac{\partial^2 \check{v}'}{\partial y^2} - \alpha^2 \check{v}'\right) - \alpha \frac{\partial^2 u_B}{\partial y^2}\check{v}' = -\frac{i}{Re}\left(\alpha^4 \check{v}' - 2\alpha_{eff}^2 \frac{\partial^2 \check{v}'}{\partial y^2} + \frac{\partial^4 \check{v}'}{\partial y^4}\right), \qquad (3.2)$$

with complex α, $\Re(\alpha)$ being the streamwise wavenumber and $\Im(\alpha)$ the streamwise amplification rate, and with complex ω, $\Re(\omega)$ being the circular frequency and $\Im(\omega)$ the temporal amplification rate.

The ordinary differential equation (3.2) is supplemented by homogeneous boundary conditions at the wall (y=0) and in the free-stream $y \gg \delta_{99}$ in which case an eigenvalue problem for the perturbation quantities is obtained, if either α or ω is assigned. We adopt the spatial approach by prescribing $\Re(\omega)$, setting $\Im(\omega)$=0 and obtain a complex disturbance spectrum α.

Due to the parallel-flow assumption, the only information required to determine stability or instability of a laminar flow is the streamwise base-flow velocity u_B at a certain streamwise location. For that reason, LST can be classified as a theory describing *local* instability. Note that for the present definition, we have an unstable flow for a given disturbance frequency $\Re(\omega)$=β=$2\pi f$, if $\Im(\alpha(u_B, \beta)) < 0$, while $\Im(\alpha(u_B, \beta)) > 0$ means that the flow is stable.

Here, a solution to the Orr-Sommerfeld equation is obtained numerically by means of an iterative shooting method (Müller 1995). Only the non-zero discrete eigenvalue corresponding to strongest amplification will be considered. Starting values for the iteration procedure are obtained from a direct solution of the temporal approach ($\Re(\alpha)$ prescribed, $\Im(\alpha)$=0), by making use of a conversion procedure based on a formula by Gaster (1962).

Application of linear stability theory to laminar separation bubbles has shown favorable agreement between theoretical results and DNS (e.g., Marxen *et al.* 2003; Marxen 2005) despite the strong non-parallelity of the base-flow profile. In most cases, only one unstable eigenmode is reported.

Velocity profiles with an inflection point are known to possess particularly large growth rates (Schlichting 1979). Profiles at separation and inside the LSB resemble free shear layers by showing such an inflection point, and thus exhibit very strong growth of small wave-like perturbations. The dominant role of the inflection point with regard to the instability in a LSB suggests this instability be attributed to the Kelvin-Helmholtz (i.e., free-shear-layer) type; this is frequently done in literature (Pauley *et al.* 1990; Watmuff 1999; Spalart & Strelets 2000; Yang & Voke 2001).

Stability diagrams for all considered base flows (cases 2.2–2.5) are computed based on linear stability theory. Results are given in Figs. 4 and 5. It can be seen that the controlled flow (cases 2.2–2.4) is more stable than the essentially uncontrolled flow (case 2.5): the amplified region (contained within the thick black line) is much smaller than in the controlled case. Such a stabilizing effect of small disturbances on the mean flow even upstream of transition was also described in Marxen (2005). Furthermore, the most unstable frequency, which roughly corresponds to f=6 in case 2.5, is lowered to $f \approx 4.5$ in cases 2.2–2.4. A shift in most unstable frequency was predicted in Marxen (2005) as an effect of the mean flow deformation.

4. Comparison of LST results with numerical simulation data

To allow for a comparison between numerical and theoretical results, numerical results are Fourier-analyzed in time using available discrete time steps I=1 to I=$\mathsf{L}_{\mathsf{per}}$

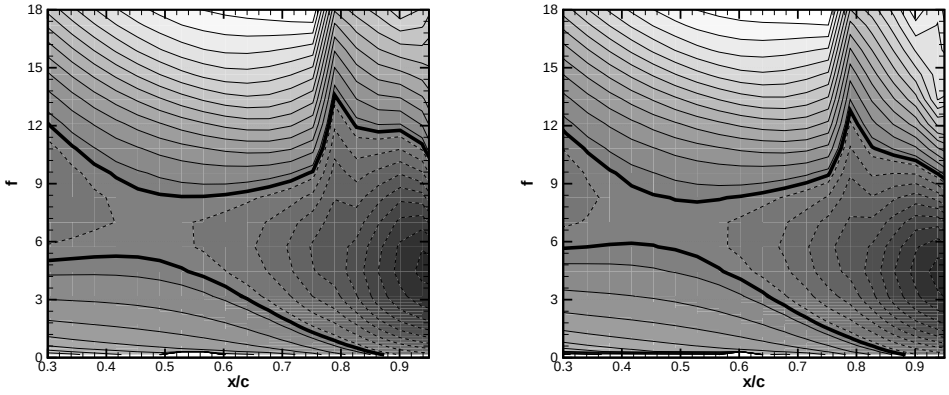

FIGURE 4. Stability diagram for cases 2.2 (left) and 2.3 (right): contours of the imaginary part of the smallest non-zero eigenvalue α_i computed from the Orr-Sommerfeld equation. The thick black line gives the contour α_i=0, while dashed lines indicate negative α_i corresponding to an amplified disturbance.

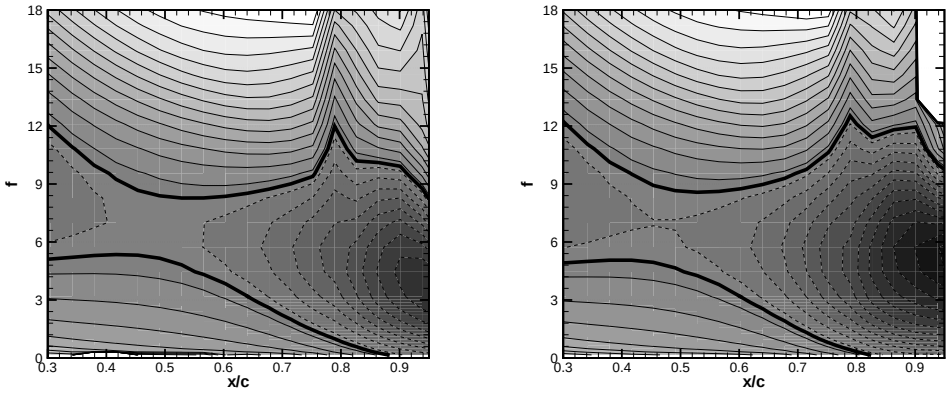

FIGURE 5. Stability diagram for cases 2.4 (left) and 2.5 (right). The legends are the same as in Fig. 4.

($\mathsf{L_{per}}$=20 . . . 25) – with the forcing frequency being the respective fundamental frequency β_0^{pp} for such an analysis. The corresponding inverse operation is Fourier synthesis, with β_0^{pp}=1.5 (case 2.2), β_0^{pp}=3 (case 2.3), β_0^{pp}=6 (case 2.4), β_0^{pp}=9 (case 2.4):

$$u(x,y,\mathsf{l}) = \sum_{\mathsf{h}=0}^{\mathsf{H}} A_u^{(f=\mathsf{h}\beta_0^{pp})}(x,y)\cos(\mathsf{h}\beta_0^{pp}\Delta t\,\mathsf{l} + \Phi^{(\mathsf{h})}(x,y)), \quad \mathsf{H} \le \mathsf{L_{per}}/2 \tag{4.1}$$

First, we compare disturbance amplification, i.e., the downstream evolution of the disturbance amplitude. For data from numerical simulations, wall-normal maxima of the amplitudes of the streamwise disturbance velocity are computed:

$$A_{u,max}^{(f=\mathsf{h}\beta_0^{pp})}(x) = max\left\{A_u^{(f=\mathsf{h}\beta_0^{pp})}(x=const,y)\right\} \tag{4.2}$$

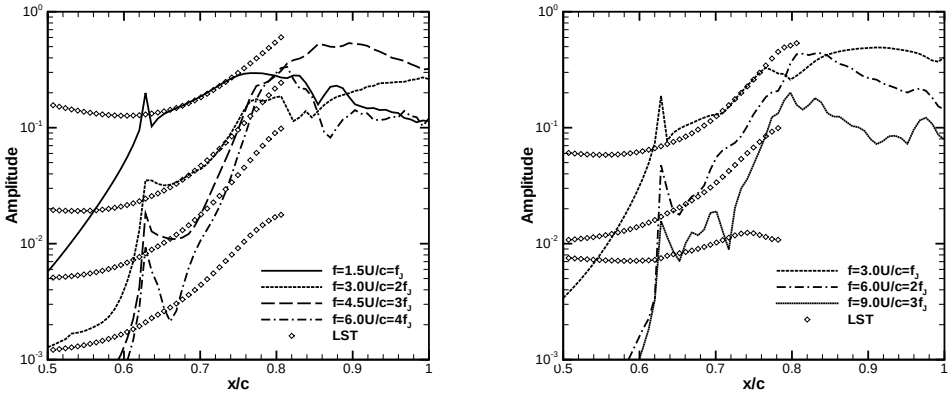

FIGURE 6. Disturbance amplification based on the streamwise disturbance velocity $A_{u,max}(x/c)$ for cases 2.2 (left) and 2.3 (right) in comparison with results from LST: $A_{LST}(x/c)$ (symbols).

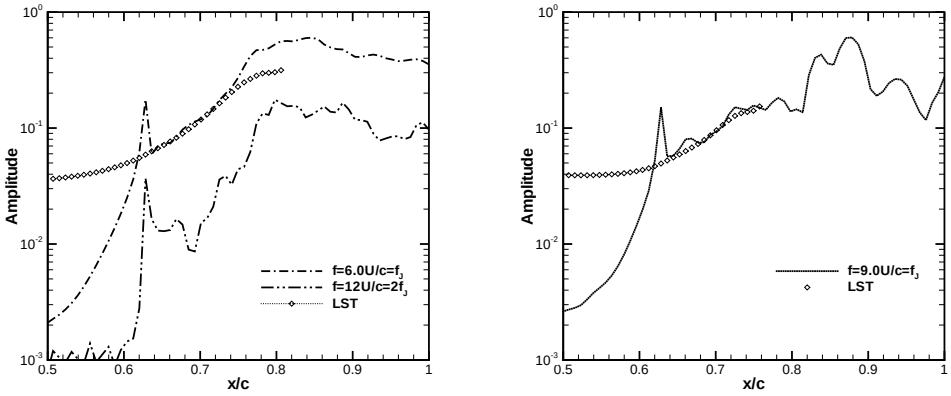

FIGURE 7. Disturbance amplification based on the streamwise disturbance velocity $A_{u,max}(x/c)$ for cases 2.4 (left) and 2.5 (right) in comparison with results from LST: $A_{LST}(x/c)$ (symbols).

These are plotted in Figs. 6 and 7. In contrast, theoretical amplification rates α_i are integrated in a downstream direction according to $A_{LST}(x/c)$=$A_0 exp(-\int \alpha_i(x/c)dx)$, all based on the respective underlying mean flow of the respective case. Since LST leaves A_0 undetermined, A_0 is chosen in an arbitrary manner for each single curve independently so that they best fit respective numerical simulation data. In all four cases the strongest peak in amplitude is visible at the position of the ZNMF actuator x/c=0.625 for the respective forcing frequency, for example for f=3 in case 2.3 (Fig. 6, right).

Furthermore, in all cases, slightly downstream of the actuator location we find a region where the observed amplification agrees well with LST for the *forced* disturbance. However, only in case 2.4 (f=6) does this disturbance also dominate the flow downstream (in the sense that it remains the largest disturbance downstream of the position of the first deviation between LST and the numerical simulation).

In case 2.2, the disturbance with f=4.5 becomes dominating downstream, and this

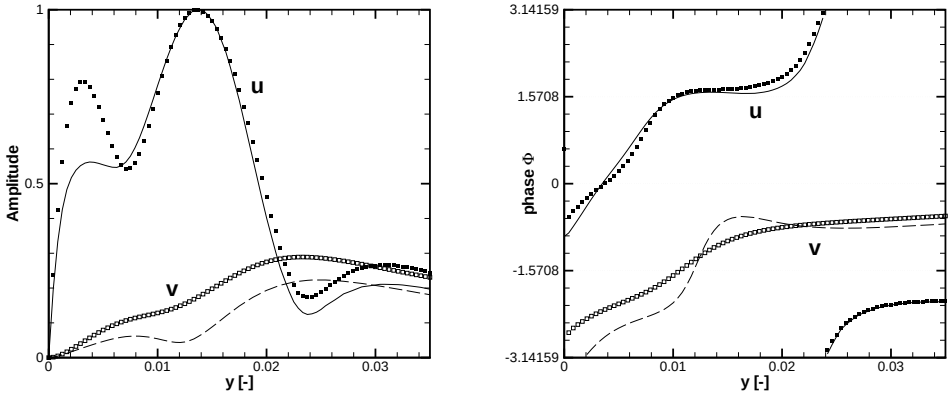

FIGURE 8. Wall-normal amplitude functions (left) and phase functions (right) for the streamwise and wall-normal disturbance velocity (amplitudes normalized by the respective maximum of the streamwise-velocity amplitude) for case 2.2, f=1.5=f_J in comparison with results from LST (symbols) at a position x/c=0.75.

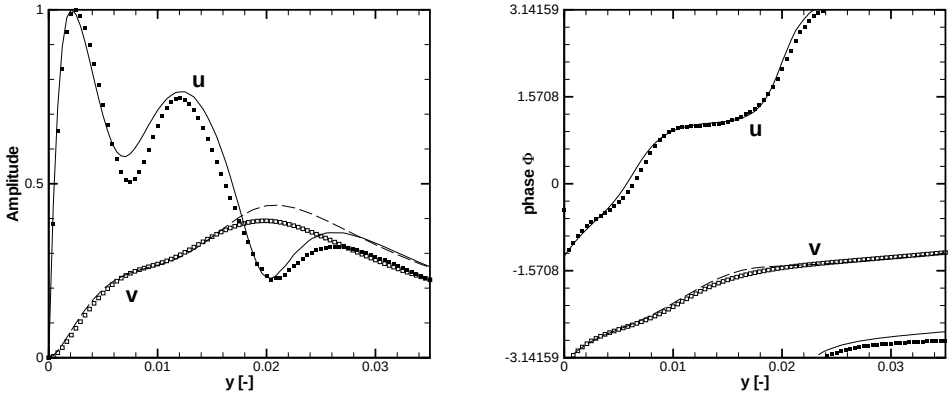

FIGURE 9. Wall-normal amplitude functions (left) and phase functions (right) for the streamwise and wall-normal disturbance velocity (amplitudes normalized by the respective maximum of the streamwise-velocity amplitude) for case 2.3, f=3=f_J in comparison with results from LST (symbols) at a position x/c=0.75.

disturbance is amplified stronger than suggested by LST (Fig. 6, left). In principal, the same is observable in case 2.3, where the disturbance with f=6 overtakes the one with f=3 at x/c=0.8 (Fig. 6, right), even though they quickly reverse order again downstream. This latter event is associated with vortex pairing, as can be seen from visualizations.

Streamwise wavenumbers computed from streamwise derivatives of the phases of the Fourier-analyzed simulation data show reasonable agreement with LST results for all four cases as well (not shown). Good agreement of numerical results with LST in all cases for the forced disturbance within a certain region downstream of actuation is confirmed by reviewing wall-normal distributions of amplitude and phase functions (see Figs. 8–11).

It appears that the lower the frequency, the more pronounced is the maximum in

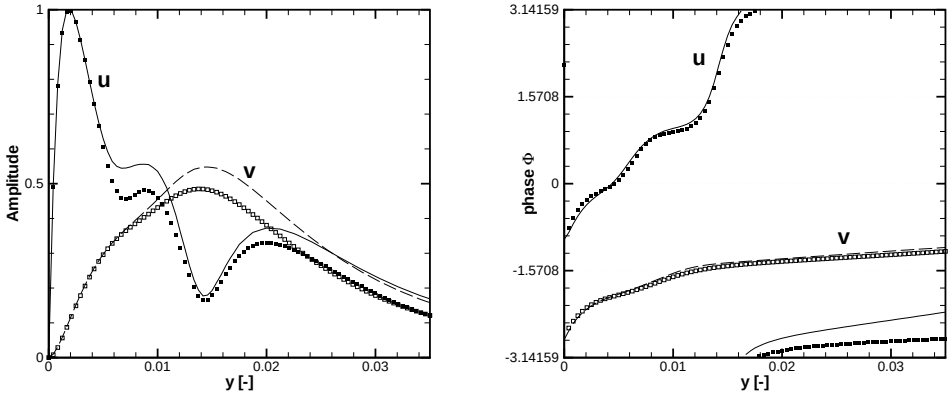

FIGURE 10. Wall-normal amplitude functions (left) and phase functions (right) for the streamwise and wall-normal disturbance velocity (amplitudes normalized by the respective maximum of the streamwise-velocity amplitude) for case 2.4, f=6=f_J in comparison with results from LST (symbols) at a position x/c=0.70.

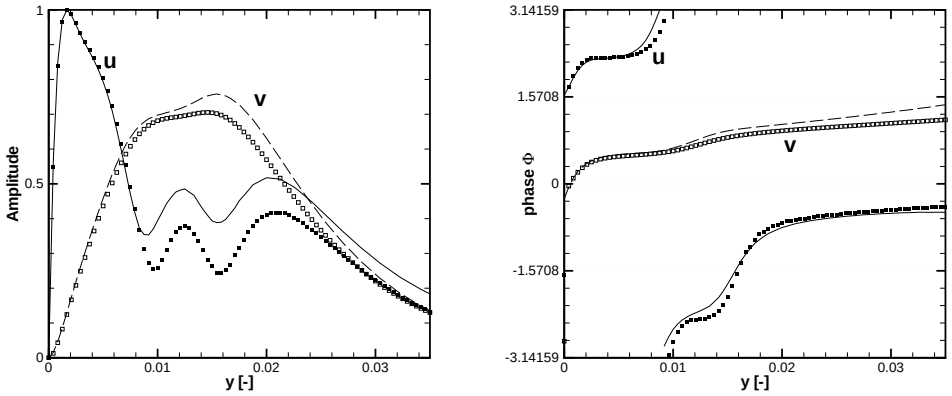

FIGURE 11. Wall-normal amplitude functions (left) and phase functions (right) for the streamwise and wall-normal disturbance velocity (amplitudes normalized by the respective maximum of the streamwise-velocity amplitude) for case 2.5, f=9=f_J in comparison with results from LST (symbols) at a position x/c=0.70.

u-amplitude away from the wall. However, keep in mind that the base flows are also different in all cases and that not the same x locations are compared (x/c=0.75 in cases 2.2 and 2.3, and x/c=0.7 in cases 2.4 and 2.5).

5. Discussion

The origin of higher harmonics (particularly visible in both cases 2.2 and 2.3, Fig. 6) is non-linear generation around the location of forcing via the ZNMF actuator. Their downstream growth is not due to a linear instability (note the poor agreement between LST and numerical results) but might be caused by continuous non-linear generation,

a secondary instability in the presence of a large fundamental disturbance, an absolute instability inside the bubble, or a global instability. Which of these possibilities is true remains unclear, but at least non-linear generation cannot explain why these initially higher harmonics finally overtake the generating one, suggesting that one of the other possibilities, i.e., instabilities, might be involved. Clarification of this issue is beyond the scope of this paper and remains a subject of further exploration in the future.

In case 2.4 we see disturbance growth of the forced perturbation in agreement with LST; this disturbance governs the flow downstream, i.e., it saturates, leading to vortex roll-up associated with gain of amplitude of higher harmonics, without letting them actually overtake, followed by vortex shedding. A similar behavior was observed in several earlier studies of transition in LSBs (e.g., Marxen 2005) and active control of LSBs (e.g., Rist & Augustin 2006). However, final disturbance growth slightly before saturation is larger compared to LST, which was not observed in the cited studies; a specific reason for this strong growth remains unclear.

Case 2.5 was denoted before as essentially uncontrolled, and from spectra given in Kotapati *et al.* (2006) it can be deduced that disturbances with frequencies lower than the forcing frequency play a significant role. These are not computable from the present data of just one forcing period. For that reason, no further conclusions about the transition process can be derived from Fig. 7. Still, we can once more observe good agreement between numerical data and LST shortly downstream of forcing, even in this case.

Disturbance saturation for the respective forcing frequency in cases 2.2 and 2.3 can be observed from the sudden drop in amplification and from deviation from good agreement with LST (Fig. 6). However, disturbances of higher frequencies in these cases grow beyond that level of saturation, unlike in case 2.4. Obviously, in cases 2.2 and 2.3 the saturation of the forced disturbance does not mark the end of the transition process, note that cases 2.2–2.4 show first saturation at roughly the same streamwise location x/c=0.76, while only case 2.4 shows an increase in Re_θ directly thereafter (even though it is soon followed by case 2.3). Moreover and more importantly, the saturation in case 2.2 does not equal quick reattachment as it does in case 2.4 (the case with the earliest reattachment). A possible explanation is that in cases 2.2 and 2.3, the forced perturbation is not able to fully transition the flow and thus the resulting (only slightly) increased mixing is not able to reattach the flow immediately. Instead, in these cases the transition process continues until it finishes with the saturation of a higher harmonic disturbance with f=4.5 (case 2.2) or f=6 (case 2.3).

In case 2.3 this continuation of the transition process is finished within a short distance, and thus both the pressure distribution and the height of the bubble in this case is quite similar to case 2.4. Also, Re_θ increases almost as early (as noted above). However, the skin-friction distribution of both cases is quite different in the rear part. This is believed to be due to the vortex-pairing mentioned earlier, which takes place in case 2.3 only: the resulting fairly large vortex that is shed from the bubble induces a large reverse-flow velocity close to the wall and causes a larger negative skin friction in the mean at the position of its formation.

So far, the influence of the finite dimension of the plate (which ends at x/c=1) was not considered; however, it could play a role with respect to the processes that remain unclear (as previously mentioned). At least in case 2.4 it is quite likely that the wake is forced by the vortices shed from the separation bubble and therefore locks on to this shedding frequency f=6 as stated in Kotapati *et al.* (2006), i.e., the wake is influenced by the bubble but not vice versa. The same seems true for case 2.3, where vortex pairing

occurs in the bubble and a vortex with frequency f=3 is shed, which again is observed as the dominating frequency in the wake. In contrast, it remains unclear what happens in the wake and whether there is interaction in cases 2.2 and 2.5.

6. Conclusions

Four different cases of a laminar separation bubble being forced at different frequencies by means of a ZNMF actuator were considered with respect to disturbance growth occurring in the respective flow. Linear instability of the resulting mean flows were evaluated based on the Orr-Sommerfeld equation, so-called local linear stability theory (LST). This led to a deeper understanding of some occurring instability processes.

Our research indicates that a larger separation bubble corresponds to a larger region of instability and a higher most-amplified frequency. A feedback effect of the mean flow deformation, i.e., a change of the mean flow caused through disturbance input even upstream of transition, could be observed in accordance with reports in Marxen (2005).

When comparing Fourier-analyzed numerical results with theoretical eigensolutions, a region of good agreement both with respect to eigenvalues (amplification rates) and eigenfunctions (wall-normal amplitude and phase functions) was found in all cases. This emphasizes that in *all* cases the ZNMF actuator triggered an instability mode in the flow.

However, the triggered instability mode was not the cause for transition in every case, nor for reattachment. Only in the case where control was most effective (case 2.4), where the forcing frequency is close to the integrally most amplified frequency of the resulting mean flow, does the triggered perturbation lead to transition and reattachment. Such a behavior is in agreement with similar studies of active flow control, e.g., Rist & Augustin (2006). Since this case also corresponds to the smallest separation bubble, it appears best for efficient flow control to select a forcing frequency close to the most amplified disturbance as computed by LST.

On the other hand, the disturbance behavior could not solely be explained in all cases by linear stability theory in the region close to transition. Instead, indications for other instabilities to be active were found and discussed, but future work is required to fully understand ongoing processes.

At least in cases 2.3 and 2.4, the cases with the second-smallest and smallest separation bubbles (based on c_p and Re_θ), the presence of a wake downstream of separation does not seem to play a role. This is due to the fact that the separation bubble dynamics are largely governed by the forced perturbation with respect to the vortex-shedding frequency, and rather this wake is just forced by the perturbations convecting downstream from the bubble. This suggests that both problems (i.e., separation bubble and wake dynamics) are decoupled and can be studied independently of each other in these cases.

Present results indicate that it would be beneficial to place the actuator further upstream, since in all cases the flow is at least neutrally stable as early as x/c=0.5 for frequencies ≥ 3. This is even more true if the most amplified frequency according to LST is selected. A drawback of LST is that it cannot predict the most amplified frequency of the *controlled* flow a *priori*. However at least an estimation can be derived from a stability analysis of the uncontrolled flow, and then a slightly lower frequency should be selected.

7. Future work

A deeper understanding of flow dynamics for the present case of laminar-separation control was gained with the help of linear stability theory. However, several questions were also raised. The following list provides an overview of possible future research on the present setup:

- The choice of the actuator length might be suboptimal (note the large drop in amplitude at the end of the slot in Figs. 6 and 7), and therefore the receptivity of the boundary layer with respect to the actuator should be investigated (varying actuator dimensions, positions, and jet exit momentum),
- The influence of the wake on the separation bubble should be clarified by simulations with a semi-infinite plate,
- Subharmonic vortex-pairing is not observed in case 2.4 (in contrast to case 2.3), a possible reason for this is the absence of a (large) subharmonic disturbance in case 2.4: a simulation with forcing at f=6 with some added smaller perturbation at f=3 could clarify the influence of subharmonic background noise on vortex pairing,
- To clarify growth of disturbances with growth rates exceeding those from LST, the flow should be investigated with respect to occurrence of (local) absolute instability, global instability, and secondary (local and global) instability.

REFERENCES

Boiko, A. V., Grek, G. R., Dovgal, A. V. & Kozlov, V. V. 2002 *The Origin of Turbulence in Near-Wall Flows*, 1st edn. Springer, Berlin, Heidelberg, New York.

Bons, J. P., Sondergaard, R. & Rivir, R. B. 2001 Turbine separation control using pulsed vortex generator jets. *J. Turbomachinery* **123** (2), 198–206.

Fasel, H. F. & Postl, D. 2006 Interaction of separation and transition in boundary layers: direct numerical simulations. In *Sixth IUTAM Symposium on Laminar-Turbulent Transition* (ed. R. Govindarajan), *Fluid Mechanics and its applications*, vol. 78, pp. 71–88. Proc. of the 6th IUTAM Symposium on Laminar-Turbulent Transition, Bangalore, India, Dec. 13-17, 2004, Springer, Berlin, New York.

Gaster, M. 1962 A note on the relation between temporally-increasing and spatially-increasing disturbances in hydrodynamic stability. *J. Fluid Mech.* **14**, 222–224.

Ham, F. & Iaccarino, G. 2004 Energy conservation in collocated discretization schemes on unstructured meshes. In *Annual Research Briefs 2004*, pp. 3–14. Center for Turbulence Research, Stanford University.

Kotapati, R., Mittal, R., Marxen, O., You, D., Kitsios, V., Ooi, A. & Soria, J. 2006 Harnessing resonant interactions for active control of separated flows. In *Proceedings of the 2006 Summer Program*, pp. 445–456. Center for Turbulence Research, Stanford University.

Marxen, O. 2005 Numerical studies of physical effects related to the controlled transition process in laminar separation bubbles. Dissertation, Universität Stuttgart.

Marxen, O., Lang, M., Rist, U. & Wagner, S. 2003 A combined experimental/numerical study of unsteady phenomena in a laminar separation bubble. *Flow, Turbulence and Combustion* **71**, 133–146.

Müller, W. 1995 Numerische Untersuchung räumlicher Umschlagvorgänge in dreidimensionalen Grenzschichtströmungen. Dissertation, Universität Stuttgart.

Pauley, L. L., Moin, P. & Reynolds, W. C. 1990 The structure of two-dimensional separation. *J. Fluid Mech.* **220**, 397–411.

Rist, U. & Augustin, K. 2006 Control of Laminar Separation Bubbles Using Instability Waves. *AIAA J.* **44** (10), 2217–2223.

Schlichting, H. 1979 *Boundary-Layer Theory*. McGraw-Hill, New York.

Schmid, P. J. & Henningson, D. S. 2001 *Stability and Transition in Shear Flows*, 1st edn. Springer, Berlin, New York.

Simens, M. P. & Jimenez, J. 2006 Alternatives to Kelvin-Helmholtz instabilities to control separation bubbles. In *Power for Land Sea and Air*, *ASME* . Proceedings of ASME Turbo Expo 2006, Barcelona, Spain, May 8-11, 2006.

Spalart, P. R. & Strelets, M. K. 2000 Mechanisms of transition and heat transfer in a separation bubble. *J. Fluid Mech.* **403**, 329–349.

Watmuff, J. H. 1999 Evolution of a wave packet into vortex loops in a laminar separation bubble. *J. Fluid Mech.* **397**, 119–169.

Yang, Z. & Voke, P. R. 2001 Large-eddy simulation of boundary-layer separation and transition at a change of surface curvature. *J. Fluid Mech.* **439**, 305–333.